Rotational stiffness of cold-formed steel roof purlin–sheeting connections

Zhao, Congxiao; Yang, Jian; Wang, Feiliang; Chan, Andrew H.c.

DOI:
10.1016/j.engstruct.2013.10.024

Document Version
Publisher's PDF, also known as Version of record

Citation for published version (Harvard):
Zhao, C, Yang, J, Wang, F & Chan, AHC 2014, 'Rotational stiffness of cold-formed steel roof purlin–sheeting connections', *Engineering Structures*, vol. 59, pp. 284-297. https://doi.org/10.1016/j.engstruct.2013.10.024

Engineering Structures 59 (2014) 284–297

Contents lists available at ScienceDirect

Engineering Structures

journal homepage: www.elsevier.com/locate/engstruct

Rotational stiffness of cold-formed steel roof purlin–sheeting connections

Congxiao Zhao [a], Jian Yang [b,c,d,*], Feiliang Wang [a], Andrew H.C. Chan [e]

[a] School of Civil Engineering, University of Birmingham, Edgbaston B15 2TT, UK
[b] School of Naval Architecture, Ocean and Civil Engineering, Shanghai Jiao Tong University, Shanghai 200240, PR China
[c] State Key Laboratory of Ocean Engineering, Shanghai Jiao Tong University, Shanghai 200240, PR China
[d] School of Civil Engineering, University of Birmingham, Birmingham, Edgbaston B15 2TT, UK[1]
[e] School of Science, Information Technology & Engineering, University of Ballarat, 3350, Australia

ARTICLE INFO

Article history:
Received 24 April 2013
Revised 8 October 2013
Accepted 14 October 2013
Available online 4 December 2013

Keywords:
Cold-formed steel
Purlin
Roof sheeting
Rotational stiffness
Connections
Analytical method
Experimental studies

ABSTRACT

Cold-formed steel (CFS) sections are commonly used in modern roof construction. Most purlin members are of thin-walled open cross section. They are usually subjected to roof loading at the top flange in either an upward or a downward direction. The load application points, where the sheeting/purlin connections are located, are often eccentric to the shear centre, and thus inevitably generate a torsional moment that will induce twisting and/or warping deformations in addition to bending deflection. This type of complexity associated with the loading conditions will be exacerbated by the occurrence of single- or mixed-mode buckling (e.g. overall, distortional and local buckling) due to compression flanges tending to move sideways. The connections between purlin and roof sheeting provide a restraining effect on purlin members by preventing such lateral and twisting movements, and thus have a beneficial effect on their load-carrying capacity. In design practice, this effect should be taken into account from a design-efficiency perspective. To this end, a key step is to quantify the rotational restraint stiffness by using an engineering-orientated model. This paper firstly reports a series of torsional restraint tests (*F*-tests) for both sigma and zed sections. Two loading directions were examined by adjusting the purlin fixing direction. The rotational angles between the connected flange and sheeting were recorded at each loading step, from which the moment–rotation curves were produced and presented for each test case. A linear relationship has been observed for the moment–rotation relationship from all test specimens. Secondly, a hand calculation model for calculating the rotational stiffness at each connection was developed. In that model, the rotation was deemed to be primarily caused by the localised deformation of the roof sheeting and the distortional deformation of the purlin flange. The rotation caused by the separation of connection was found to be negligible. The model was validated by the experimental test results and an example was presented to demonstrate the application of the model proposed. The rotational stiffness calculated by this model can be used to evaluate the input parameters required for numerical modelling of purlin–sheeting interaction.

1. Introduction

Cold-formed steel (CFS) sections have a wide range of applications in modern construction, such as being used as purlins or as side rails in light-weight buildings [1]. For building structural systems, a purlin is a type of secondary element acting as an intermediate member in the load path to transfer load from the roof sheeting to the primary frame structure. Common types of purlin sections include channel, zed and sigma shapes. In design practice, this group of sections is normally classified as slender because the sections are unlikely to reach their full cross-sectional resistance governed by the yield stress of constituent material [2]. Furthermore, the open and thin-walled cross sections may lead to a high susceptibility to various types of buckling failure, e.g. local, distortional and lateral torsional buckling. Roof sheeting, which is normally attached to purlins using self-drilling screws, can enhance a purlin's load resistance by supplying it with a certain degree of lateral and rotational restraining effect. Therefore, it is common and economical to treat these two members as an interactive system during the design process [3].

Research into the performance of purlin–sheet systems can date back to the 1960s, including some key research studies mentioned

* Corresponding author at: State Key Laboratory of Ocean Engineering, Shanghai Jiao Tong University, Shanghai 200240, PR China; School of Naval Architecture, Ocean and Civil Engineering, Shanghai Jiao Tong University, Shanghai 200240, PR China. Tel.: +86 13917654726.
E-mail addresses: cxz666@adf.bham.ac.uk (C. Zhao), j.yang.3@bham.ac.uk (J. Yang), fxw150@adf.bham.ac.uk (F. Wang), a.chan@ballarat.edu.au (A.H.C. Chan).
[1] On leave.

0141-0296/$ - see front matter © 2013 Elsevier Ltd. All rights reserved.
http://dx.doi.org/10.1016/j.engstruct.2013.10.024

Nomenclature

a	the distance between the screw and the line of contact between purlin and sheeting	I_s, I_p	the second moment of areas of sheeting and purlin
b	the remaining flange width after subtracting a, i.e. $C - a$	θ_s	the rotation angle of the cantilever sheet at the screw connection
b_T	the breadth of the single trough of roof sheeting	θ_l	the rotation angle associated with the localised deformation of the sheet at the screw connection
C	the flange width	θ_k	the rotation angle due to the separation between the roof sheet and the purlin flange at the screw connection
C_d	the rotational stiffness	θ_p	the rotation angle due to the purlin flange bending
D	the bending stiffness of roof sheeting per unit run, $Et_s^3/12(1-\nu^2)$		

below. Lucas et al. [4,5] initially presented a full, and later a simplified, finite element (FE) model to study the interactional behaviour and its effect on the load-carrying capacity of purlin–sheet systems. The full FE model was comprehensive and accounted for both gravity and uplift loading conditions; however, not all modelling information was presented in detail and hence the model is difficult to reproduce. Vieira et al. [6,7] developed an FE model for the purlin–sheeting system, allowing for the material and geometric nonlinearity effects, to investigate the ultimate load and the longitudinal stress in channel shaped purlins. Li et al. [8] has presented an analytical method for predicting the flexural behaviour of zed purlins under uplift load when they are partially restrained by roof sheets. The model adopts the classic asymmetrical beam theory by considering both bending and twisting effects. Research by Sokol [9] focused on the lateral torsional buckling of purlins restrained by sheeting, and developed a semi-analytical method taking into account the effects of anti-sag bars and the moment gradient. All these studies concur that roof sheeting provides both lateral and rotational restraint to purlins. While the lateral restraint is usually considered to be fully effective, the rotational restraint can be variable but plays a vital role in determining the flexural behaviour of purlins [10], e.g. a higher rotational stiffness can lead to a reduced buckling length in the compression zone, a reduced tensile stress in the free flange, and therefore a higher loading resistance [11].

There is a consensus that the effect of rotational restraint of purlin–sheeting systems is associated with a variety of factors such as the shape and thickness of the sheeting, the geometry of the purlin, the number of screws per unit length, and the type of screw and its applied location. Ye et al. [12,13] investigated the effect of the magnitude and location of rotational restraints on buckling

Table 1
Nominal cross section dimensions for sigma sections.

Section code	Depth (mm)	Flange (mm)	Lips (mm)	Outer-web (mm)	Stiffener (mm)	Thickness (mm)
Σ20012	200	62.5	20	45	16	1.2
Σ20016	200	62.5	20	45	16	1.6
Σ20025	200	62.5	20	45	16	2.5
Σ24015	240	62.5	20	45	16	1.5
Σ24023	240	62.5	20	45	16	2.3
Σ24030	240	62.5	20	45	16	3.0
Σ30018	300	75.0	20	60	16	1.8
Σ30025	300	75.0	20	60	16	2.5
Σ30030	300	75.0	20	60	16	3.0

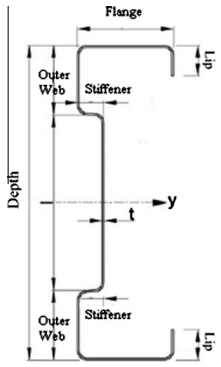

y–y is geometric axes of cross section.

Table 2
Nominal cross section dimensions for zed sections.

Section code	Depth (mm)	Flange (mm)	Lips (mm)	Thickness (mm)
Z14614	145	62.5	20	1.4
Z14618	145	62.5	20	1.8
Z20618	200	65	20	1.8
Z30720	300	75	20	2.0

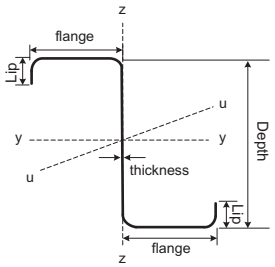

y–y is geometric axes *u–u* is principal axes of cross section

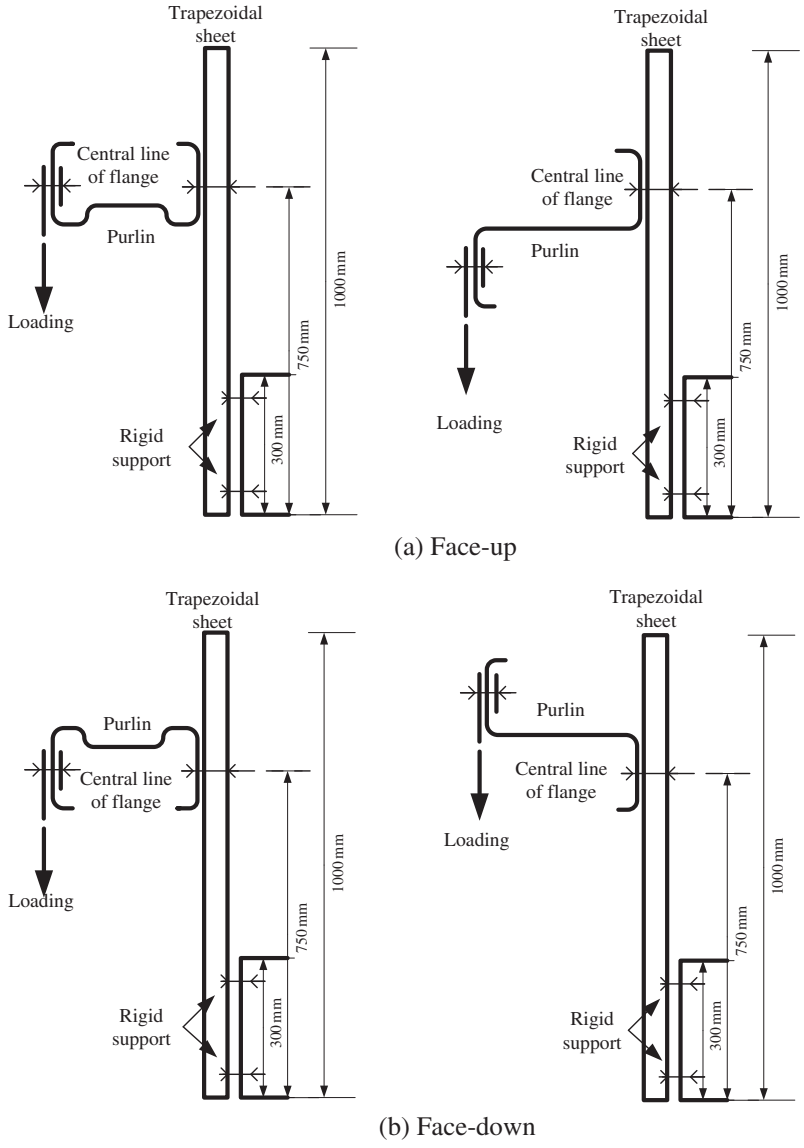

Fig. 1. Test set-up for sigma and zed sections.

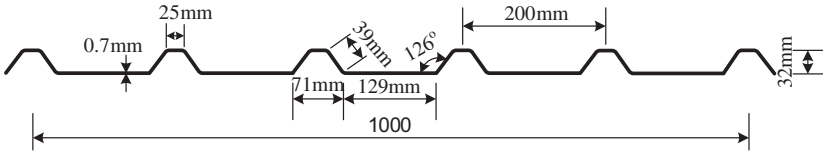

Fig. 2. Dimensions of the roof sheet.

resistance and the buckling mode of purlins. The study from Schafer [14] indicates that an adequate rotational restraint from roof sheeting can partially or even fully eradicate the distortional buckling failure mode. Fiorino et al. [15] carried out an experimental study on the effect of screw connections on the behaviour of the roofing system by considering various sheathing types, loaded edge distances and loading conditions. Katnam et al. [16,17] presented a nonlinear FE model to quantify the rotational stiffness of both single-skin and insulated sandwich sheeting. Vrany [18] adopted a flexibility method to predict rotational stiffness at connection. The numerical model took account of most influencing factors, and hence it became overly complicated and the derivations of some coefficients were unclear.

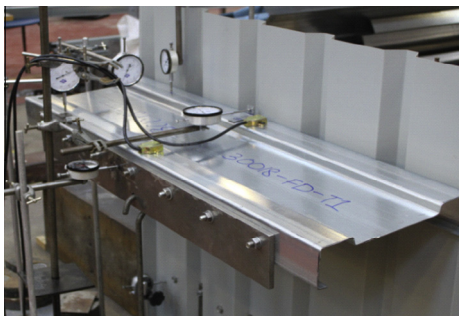

Fig. 3. Multiple point loads to simulate the uniformly distributed load (UDL).

In design practice, the current numerical model adopted in EC3 [19] for determining rotational stiffness was first introduced by Lindner and Gregull [20], who considered the stiffness into three parts: that due to the out-of-plane flexural stiffness of the sheeting, the purlin's resistance to distortion, and the localised deformations at the connection point. The coefficients in the empirical equations were derived from extensive test data, in which assumptions were made to simplify the problem, but they often led to overly conservative outcomes. The *R*-factor approach is adopted by the North America Notification [21], which takes account of the effect of rotational and lateral stiffness into a reduction factor. This design method is user-friendly, but the detailed deduction procedure for corresponding *R*-factors is unclear.

A closed-form engineering model for rotational stiffness is required for the task of predicting sheeted roof purlin resistance within European design standards (EC3). The semi-analytical model developed by Gao and Moen [22] is to date the latest and most accurate method. The model considers the rotation at connections generated by both localised deformation of a panel and the bending of a restrained purlin flange. The model distinguishes channel and zed sections and provides results of less than 11% deviation in comparison to experimental studies and FE simulations. However, the method has some limitations:

(1) The method assumes only one type of contact for zed and channel sections under the uplift loading condition. It is valid for channel sections since the torsional moment caused by the eccentric applied load brings the section into contact with the roof sheet at its flange-lip junction line. However, according to Vrany [10], there are two possible deformation modes for zed sections. Depending on the direction of the eccentric load, the purlin may be in contact with the attached sheet at either the flange-web or the flange-lip junction line. Therefore, this will lead to different behaviour patterns in the resulting rotational stiffness.
(2) The method utilises a rather simplified FE model that neglects purlin–sheeting interaction at the screw points; hence to obtain results, engineers need to have access to computer programmes.

(a) Dial gauges and inclinometers attached to purlin

(b) Dial gauges placed at the rear side of the roof sheet

Fig. 4. Measurement of displacements.

Table 3
F-test results.

Specimen ID	Measured web depth (mm)	Measured purlin thickness (mm)	Load[a] (N)	Rotation, radian	Vertical deformation (mm)	C_d (N mm/rad/mm)
Σ20012FD	203	1.26	141	0.072	21.5	394
Σ20012FU	201	1.23	151	0.054	19.5	502
Σ20016FD	200	1.58	201	0.070	21.5	622
Σ20016FU	200	1.62	241	0.070	21.7	691
Σ20025FD	200	2.40	328	0.073	21.8	895
Σ20025FU	198	2.42	384	0.075	20.8	1024
Σ24015FD	239	1.58	151	0.063	23.4	593
Σ24015FU	241	1.58	151	0.052	24.5	696
Σ24023FD	241	2.17	301	0.085	24.0	848
Σ24023FU	241	2.20	301	0.072	23.6	1009
Σ24030FD	240	2.95	385	0.091	22.7	909
Σ24030FU	241	2.99	381	0.087	22.6	1047
Σ30018FD	301	1.81	201	0.082	30.9	735
Σ30018FU	301	1.79	171	0.068	29.8	753
Σ30025FD	300	2.37	241	0.079	30.8	921
Σ30025FU	301	2.31	301	0.084	29.5	1078
Σ30030FD	301	3.04	341	0.105	30.8	977
Σ30030FU	302	2.99	381	0.096	30.5	1191
Z14614FD	147	1.56	302	0.086	14.2	512
Z14614FU	145	1.54	331	0.061	13.5	762
Z14618FD	145	1.78	404	0.080	14.9	730
Z14618FU	147	1.78	444	0.078	14.9	820
Z20617FD	200	1.80	261	0.077	21.3	680
Z20617FU	202	1.71	320	0.073	19.3	876
Z30720FD	299	2.08	221	0.084	31.2	791
Z30720FU	300	2.08	261	0.082	29.5	955

[a] These recorded loads cause the vertical deflection of the free flange of purlin equal to approximately 1/10 of the purlin web depth.

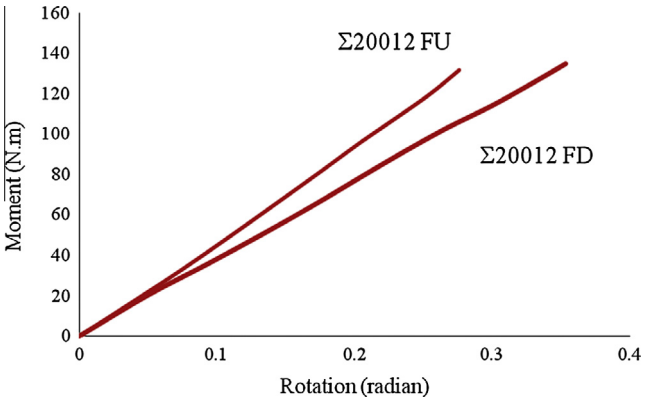

Fig. 5. A typical moment–rotation curve of Σ20012.

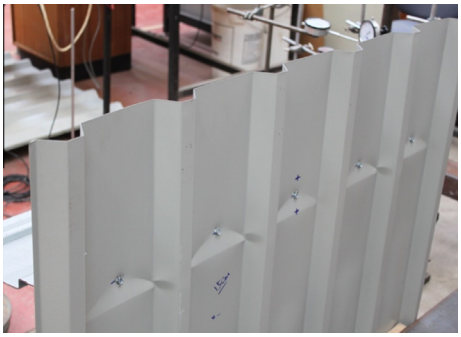

Fig. 6. Local plastic deformation of sheet.

(3) Validation shows that this model is not suitable for specimens outside the specified range, which suggests that the panel's local bending stiffness provided in the paper may be calibrated for the tested specimens only.

In this paper, an analytical model is developed for predicting the rotational restraint stiffness of Grade S450 purlins connected to roof sheeting by using self-drilling screws. The model takes account of purlin–sheeting interaction and the effect of loading directions by considering the rotational stiffness being contributed by the localised bending of the roof panel and the bending of the purlin flange panels at the connection point. This analysis is based on Kirchhoff thin plate theory. A series of rotational restraint tests (*F*-test) were conducted and the results were used to validate the analytical model.

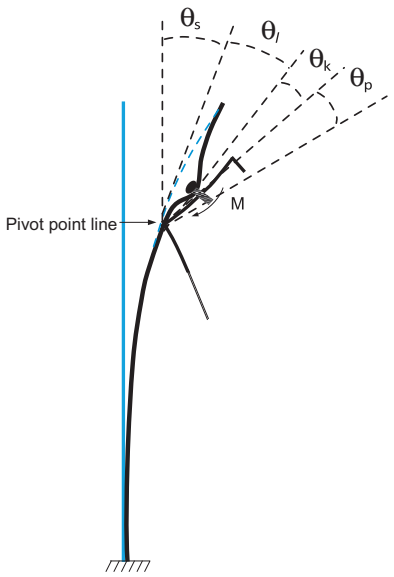

Fig. 8. Rotation developed during the *F*-test.

2. Experimental study (*F*-test)

2.1. Test specimens

CFS zed and sigma purlin sections provided by Albion Sections Ltd. were used as test specimens. Geometric information is summarised in Tables 1 and 2, respectively. The nominal yield stress of the tested specimen is 450 N/mm^2. In this test program, each specimen is assigned with a unique three-part ID indicating the purlin type, cross-sectional dimensions (represent the web depth and the thickness) and purlin directions ("facing down" or "facing up" represents the uplift and gravity loading conditions and are denoted as FD or FU hereafter, respectively). For example, specimen Σ20025FD indicates a sigma section with a web depth of 200 mm and cross sectional thickness of 2.5 mm, which is fixed in a "facing down" manner.

2.2. Test set-up and instrumentation

Torsional restraint tests (*F*-test) adapted on the basis of EC3 guidance [19] were carried out for purlin profiles connected to roof sheets in order to estimate the rotational stiffness under both uplift and downward loading conditions. The test set-up is shown in

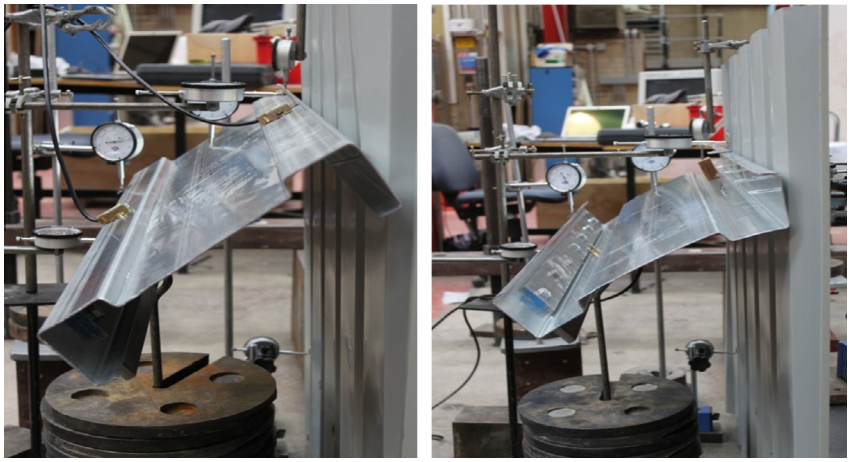

Fig. 7. Deformation modes for both FD and FU specimens.

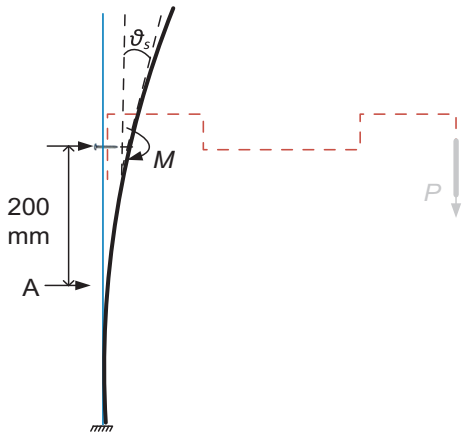

Fig. 9. Cantilever sheet in the test and the calculation model.

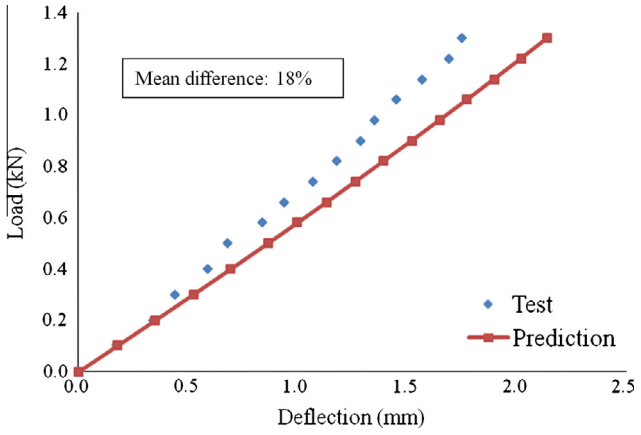

Fig. 10. Comparison of the load–deflection between test and prediction for Σ24015FU.

Fig. 1. A single-skin trapezoidal roof sheet with dimensions of 1070 × 1000 × 0.7 mm was fixed onto a hot-rolled steel channel section with two rows of bolts at the centre of each trough. Timber blocks and steel plates were also used to clamp-fix the base. Such fixing configuration aims at forming a rigidly supported cantilever system. The dimensions of the roof sheet profile are presented in Fig. 2.

A purlin section of 1000 mm length was through-fastened to every sheet trough by self-drilling screws on the central line of the purlin flange. Neoprene washers were used to prevent water leaking at connections. The effect of loading direction was examined by adjusting the purlin fixing direction, ie. the purlin was facing up under gravity loading so that purlin–sheeting contact took place at the flange-web junction line, and it was facing down under the uplift loading so that the contact took place at the flange lip conjunction line.

A stiff steel plate was bolted to the free flange of the purlin by using several bolts to simulate the load distribution; weights were applied to this steel plate by using a hook (Fig. 3). As a result of such a loading arrangement, the load applied by the weights was always in the vertical direction. Weights were applied in increments until the occurrence of plastic deformation in the roof sheet. The vertical deflections at several locations were recorded at each loading increment by using dial gauges, which were placed at the purlin's outer webs and free flange (Fig. 4a). The rotational angles near both restrained and free flanges were monitored by using two digital inclinometers, with an accuracy of 0.1°, placed at the outer webs as close to the web-flange junction lines as possible. The lateral displacements of sheet and purlin due to bending were recorded (Fig. 4b).

2.3. F-test results

Tests were continued until the yield failure of roof sheeting occurs. The applied load and deflections were recorded at each loading increment, from which a complete moment against rotation relationship for each screw connection can be established. Table 3 presents a summary for the actual sizes of test specimens, the loads that cause the vertical deflection of the free flange of purlin

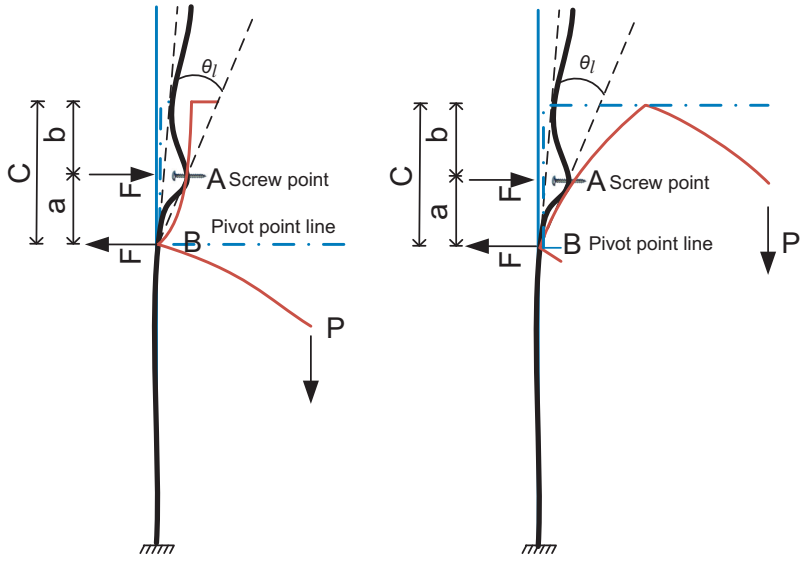

(a) Contact at flange-web line (b) Contact at flange-lip line

Fig. 11. Purlin–sheet interaction at a connection point.

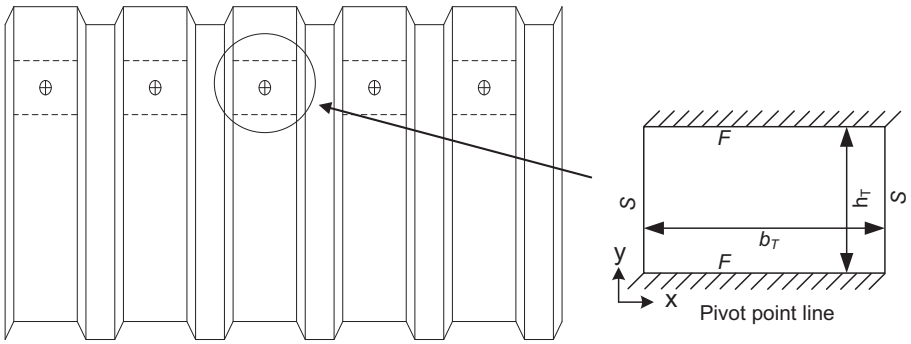

Fig. 12. Plate model for predicting rotation due to localised sheet deformation.

Table 4
Typical values of coefficient β.

Screw location in the trough	b_T/h_T ratio							Regression equations
	1.0	1.2	1.4	1.5	1.6	1.8	2.0	
At centre	0.077	0.078	0.078	0.078	0.078	0.077	0.077	$\beta = 0.078$
At 1/3 trough width	0.057	0.055	0.051	0.049	0.046	0.042	0.037	$\beta = -0.003\frac{b_T}{h_T} + 0.061$
At 1/4 trough width	0.043	0.040	0.035	0.032	0.029	0.024	0.020	$\beta = -0.004\frac{b_T}{h_T} + 0.047$
At 1/5 trough width	0.034	0.031	0.026	0.024	0.022	0.017	0.014	$\beta = -0.003\frac{b_T}{h_T} + 0.038$
At 1/10 trough width	0.017	0.015	0.012	0.010	0.009	0.006	0.004	$\beta = -0.002\frac{b_T}{h_T} + 0.019$

Note: the values derived in Table 4 are for t_s of 0.7 mm, for different thickness use $\beta' = \frac{\beta t^3}{0.7^3}$.

equal to approximately 1/10 of the purlin web depth, the rotation and vertical deformation measured at this load level. The rotational stiffness C_d of each specimen was determined by dividing the moment induced at connection due to that vertical load by the corresponding rotation captured, and is also presented in the same table. This approach of calculating the rotational stiffness is in accordance to the requirement by EC3-1-3 [19].

Typical complete moment–rotation curves recorded for specimen Σ20012 are presented in Fig. 5 for both FU and FD arrangements; similar curves for other specimens are presented in Fig. 15 (later in the paper) in comparison to the theoretical prediction results. A common feature of these curves is that they remain almost linear during the entire loading range. The yield moment ranges from 93 N m for Z14614 specimen to 300 N m for Σ30030 specimen. Failed specimens were unloaded and dismounted and the permanent deformation was revealed. It can be seen from Fig. 6 that by the end of loading, localised plastic deformation occurs at each screw connection point, as evidenced by noticeable yield lines formed along the contact line, and two lines linking the screw point to both ends of the contact line. In all tests, the purlin sections have a greater thickness than the roof sheet. Distortional deformation of the purlin can only be clearly observed at the time the plastic yield line is about to be formed. Typical deformation modes of the tested purlin–sheeting system observed during tests are presented in Fig. 7 for both face-down and face-up tests.

3. Analytical model

An analytical model is developed and presented here for predicting the rotational stiffness of the purlin specimen at connection points under the applied loads as seen in the test. The purlin is connected to the roof sheet with self-drilling screws at one flange, but is free to move at the other flange. The total rotation angle captured near the junction line between the connected flange and the adjacent outer web (pivot point line) should comprise the following four components, illustrated in Fig. 8 and summarised as:

(1) θ_s, the rotation angle of the cantilever sheet under a row of concentred moments generated at screw connection points; (2) θ_l, the rotation angle associated with the localised deformation of the sheet under the pulling force in each screw; (3) θ_k, the rotation angle due to the separation of the roof sheet and the purlin flange at the connection point; and (4) θ_p, the rotation angle due to the purlin flange bending.

In Fig. 8, the vertical load applied at the free flange is omitted but is replaced by a concentrated moment at the connection point as a result of it.

3.1. Rotation angle of the cantilever sheet, θ_s

During the *F*-test, the trapezoidal sheet is rigidly fixed at the base and free at the top, behaving as a cantilever one-way plate. The loaded purlin section transfers the load to the sheet in the form of a row of concentrated moments, which produces rotation angle

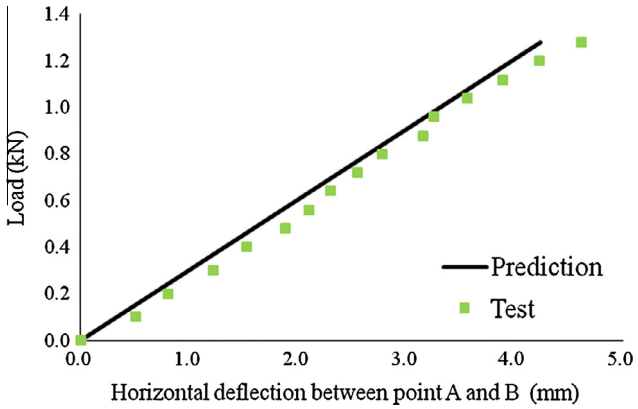

Fig. 13. Comparison of load-localised deflection between test and prediction for specimen Σ30018FU.

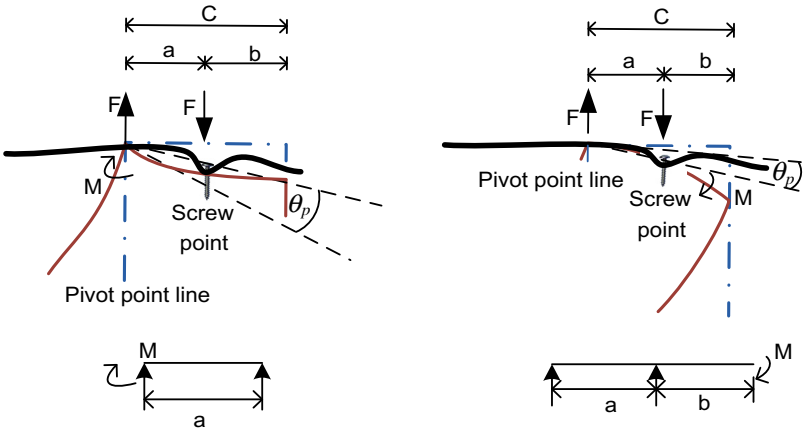

(a) Contact at the purlin's flange-web junction line

(b) Contact at the purlin's flange-lip junction line

Fig. 14. Analytical model of rotation angle caused by purlin flange bending.

θ_s (Fig. 9). The magnitude of θ_s depends on the geometric configuration and the fixing arrangement of the sheet and the applied moment. Therefore the rotation stiffness associated with this component varies with actual construction details and should be considered separately. In this case, it will be excluded from the overall rotation angle measured from the inclinometer. It is anticipated that the real rotation of the cantilever sheet should be very close to the theoretical calculation based on the cantilever theory. To confirm this, we also included a horizontally placed dial gauge at 200 mm below the screw point to measure the lateral deflection (point A in Fig. 9). The measured deflections at point A were then compared with the calculated ones based on the one-way cantilever plate. The comparison of an example of Σ24015FU is presented in Fig. 10, which shows a reasonably close agreement. The calculation follows $\theta_s = ML_1/EI_s$, where L_1 is the vertical distance between the fixed support and the connection point, and EI_s is the flexural rigidity of the sheet. The reason that the measured behaviour of the roof sheet is stiffer than the calculation model, as shown in Fig. 10, is due to there being a concentrated line load induced by the contact line between the purlin flange and roof sheeting. This load produces a localised deformation in the sheet, which is opposite to the cantilever deflection. The deflection recorded at point A, therefore, will be smaller than the pure cantilever case. However, since the rotation caused by this effect is insignificant compared to other components, it is deemed that the proposed theoretical prediction is acceptable.

3.2. Rotation angle caused by the localised deformation of sheet at connection, θ_l

To retain the moment equilibrium, a couple is induced at each purlin–sheeting connection point, with two opposite-and-equal forces F acting at the screw point and the line of contact, respectively. While the reaction force at the line of contact is supported by the webs of the roof sheet, the pulling force from the screw will produce a localised deformation in the sheet in the surrounding area and the rotation angle due to this local deflection is defined as θ_l (Fig. 11).

The conversion between F and M can be achieved as $F = M/na$, where F is the applied force per unit area, a is the distance between the screw and the line of contact and n is the number of screws. In this case, since the screw is applied at the mid-point of the purlin flange, a equals the half flange width, C. This load causes the roof sheet to deform locally around the screw point. Assuming the force at each screw point is identical, the deformation of the sheet at every trough can be treated as a thin rectangular plate subjected to a concentrated load (Fig. 12). By adopting the classic Kirchhoff thin plate theory [23], the governing equation can be expressed as:

$$\left(\frac{\partial^2}{\partial x^2}+\frac{\partial^2}{\partial y^2}\right)^2 w = \frac{F}{D} \tag{1}$$

where w is the deflection of the plate and D is the bending stiffness, i.e. $Et_s^3/12(1-\nu^2)$, E is the Young's modulus of the plate material, and t_s is the thickness of the roof sheet.

In line with the deformation pattern, the boundary conditions can be set as follows: two vertical folding lines of the sheet are considered as simply supported (S). The pivot point line is considered as the fixed edge (F) due to the observation of a very early occurrence of plastic hinge under the applied load. A hypothetical line is chosen at a zero deflection location as the fourth line, also considered as fixed (F). Therefore the final boundary conditions along with the dimension symbols are illustrated in Fig. 12, where b_T is the sheet trough width; and h_T is the height of the plate where fixed edges are located; in this case it can be assumed to be equal to the purlin flange width C.

A Levy's solution can be obtained for w (see Appendix A). To facilitate the engineering application, the solution can be simplified into the following form:

$$\theta_l = \frac{w}{a} = \frac{\beta F h_T^2}{Et_s^3 a} = \frac{\beta M h_T^2}{nEt_s^3 a^2} \tag{2}$$

where M is the moment applied at the connection by the vertical load P. The coefficient β depends on the b_T/h_T ratio and the location of the screw in relation to the trough panels. For ease of design purposes, common values of β are presented in Table 4.

To validate this model, the horizontal displacement at points A and B were measured (see Fig. 11). The differential displacements between these two points were calculated and compared with the calculation results. A comparison of specimen Σ30018FU is presented in Fig. 13 with total applied load plotted against horizontal difference between point A and B, which shows a close agreement.

3.3. Rotation angle caused by the separation of connection, θ_k

Under the applied load, the purlin profile tends to separate from the sheet due to the resilience of the sealing washer. In our tests, it

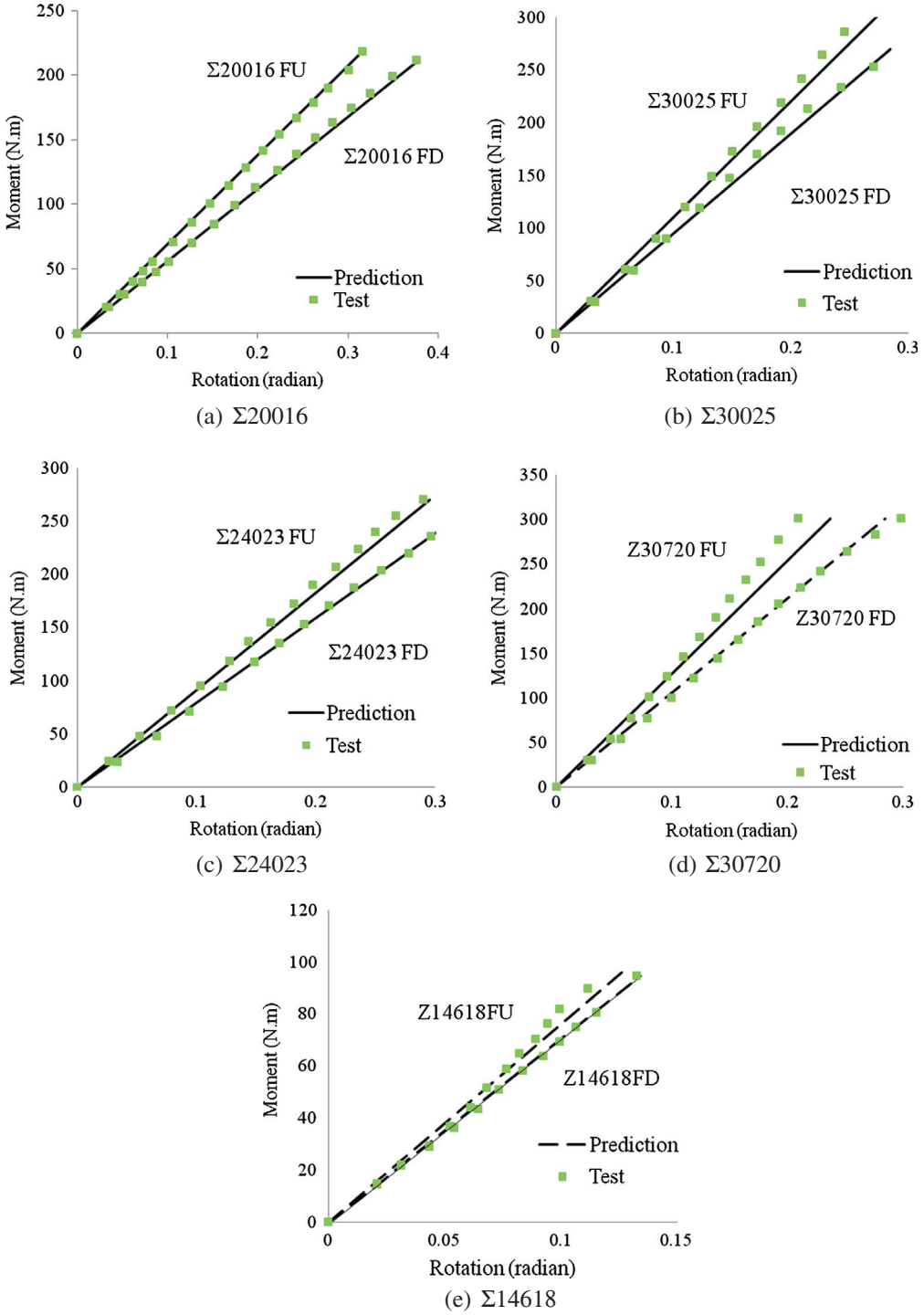

Fig. 15. Moment–rotation relationships between test results and analytical predictions.

has been found during the linear stage that the rotation associated with this effect is relatively small compared to the other components. Therefore this component is ignored in the calculation model.

3.4. Rotation angle caused by the deformation of purlin flange, θ_P

The deformation of the purlin flange and web is calculated with the bending theory for one way slabs. By rotating Fig. 11 by 90°, the flange panel between the pivot line and screw point, as illustrated in Fig. 14, can be assumed as a simply supported one-way plate with a moment applied at one end. Thus the maximum rotation can be expressed in Eqs. (3a) and (3b) depending on the contact:

$$\theta_P = \frac{Ma}{3EI_P} \tag{3a}$$

$$\theta_P = \frac{Ma}{3EI_P} + \frac{Mb}{EI_P} \tag{3b}$$

where a is the vertical distance between the screw point and the line of contact, and EI_p is the flexural rigidity of the purlin flange panel. It has been suggested that the contact conditions under differ-

Table 5
Comparisons of rotational stiffness between test and analytical predictions.

Specimen name	C_d prediction (N m/rad/m)	C_d test (N m/rad/m)	Test/prediction ratio	Average C_d	FD/FU ratio
Σ20012 FD	403	394	0.98	399	0.79
Σ20012 FU	508	502	0.99	505	
Σ20016 FD	607	622	1.02	615	0.78
Σ20016 FU	772	691	0.89	732	
Σ20025 FD	930	895	0.96	913	0.89
Σ20025 FU	1048	1024	0.98	1036	
Σ24015 FD	588	593	1.01	591	0.80
Σ24015 FU	731	696	0.95	714	
Σ24023 FD	860	848	0.99	854	0.87
Σ24023 FU	987	1009	1.02	998	
Σ24030 FD	939	909	0.97	924	0.86
Σ24030 FU	1090	1047	0.96	1069	
Σ30018 FD	672	735	1.09	704	0.83
Σ30018 FU	805	753	0.94	779	
Σ30025 FD	883	921	1.04	902	0.88
Σ30025 FU	1002	1078	1.08	1040	
Σ30030 FD	1023	977	0.96	1000	0.92
Σ30030 FU	1108	1191	1.07	1150	
Z14614 FD	557	512	0.92	535	0.72
Z14614 FU	717	762	0.94	740	
Z14618 FD	723	730	1.01	727	0.81
Z14618 FU	889	820	0.92	855	
Z20617 FD	674	680	1.01	677	0.78
Z20617 FU	868	876	1.01	872	
Z30720 FD	810	791	0.98	801	0.85
Z30720 FU	958	955	1.00	957	

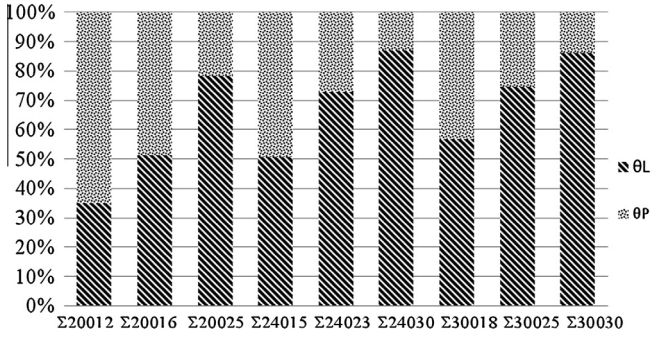

Fig. 16. Proportion of θ_l and θ_p in the overall rotation under the FD condition for sigma sections.

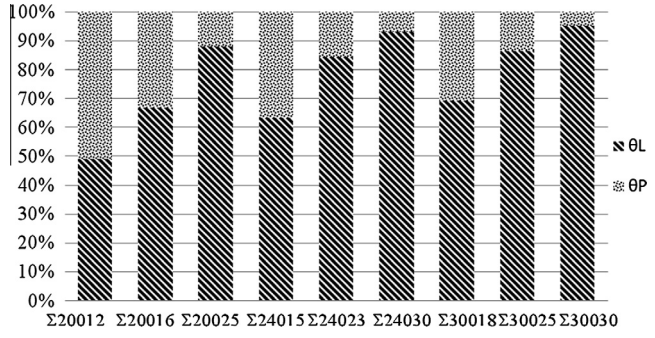

Fig. 17. Proportion of θ_l and θ_p in overall rotation under the FU condition for sigma sections.

ent loading directions can be determined for channel and sigma sections, i.e. a flange-web junction line contact for the gravity load and a flange-lip junction line contact for the uplift load. However, for zed sections under a specified loading direction, the purlin flange may be in contact with the sheet in either way, depending on factors such as the screw position, purlin geometry and the loading magnitude [18].

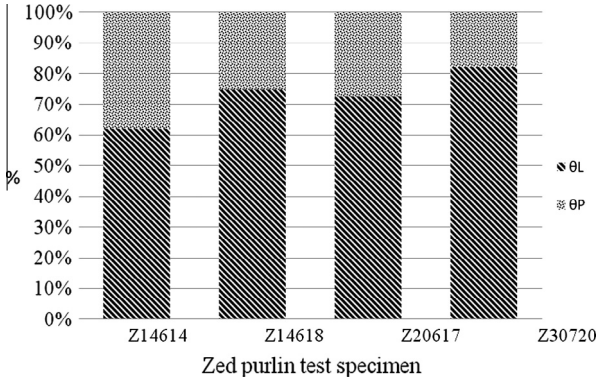

Fig. 18. Proportion of θ_l and θ_p in overall rotation under FD condition for Z sections.

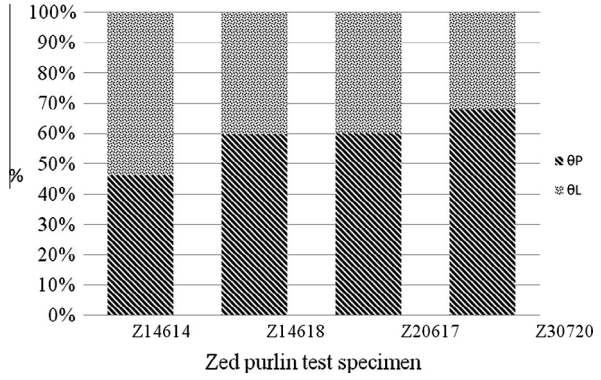

Fig. 19. Proportion of θ_l and θ_p in overall rotation under FU condition for Z sections.

Based on the abovementioned assumptions and validations, it can be suggested that the terms of θ_l and θ_p are considered in our analytical model. The term of θ_s should be determined based on the actual construction design details and by using the one-way slab theory. The term of θ_k is deemed to be negligible. The final

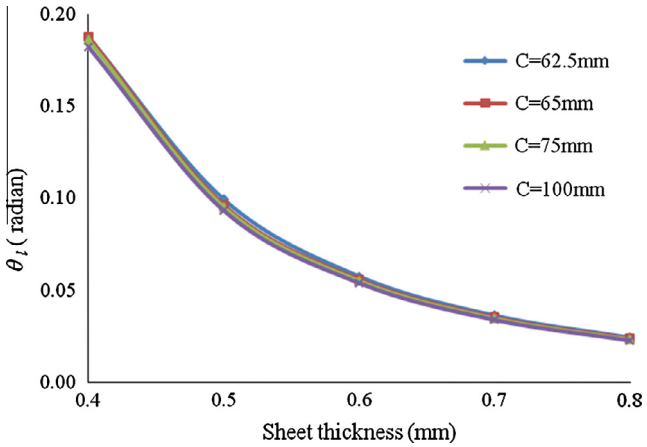

Fig. 20. Relationship of θ_l with sheet thickness under different flange widths *C*.

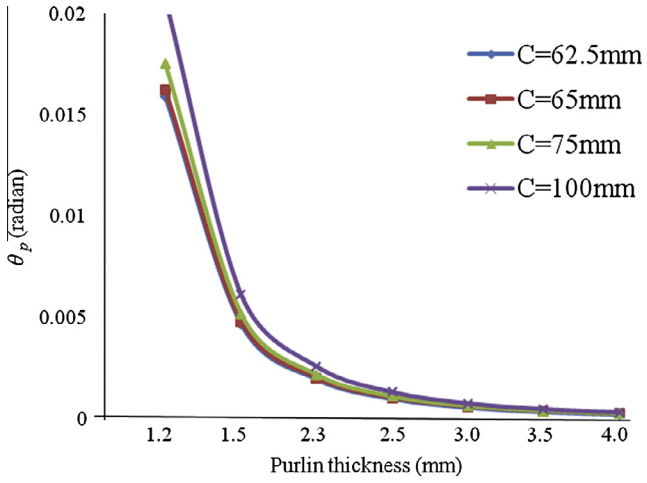

Fig. 21. Relationship of θ_p with purlin thickness under different flange widths, *C*.

rotational stiffness per unit length run at each connection, i.e. C_D, with a unit of N mm/rad/mm, can be expressed as:

$$C_D = \frac{M}{\theta_L + \theta_P} = \frac{M}{\left(\frac{\beta M h_T^2}{n E t_s^3 a^2} + \frac{Ma}{3EI_p}\right)} = \frac{E}{\left(\frac{\beta h_T^2}{n t_s^3 a^2} + \frac{a}{3I_p}\right)} \quad (4)$$

when the contact is at the flange-web junction line; and

$$C_D = \frac{M}{\theta_L + \theta_P} = \frac{M}{\left(\frac{\beta M h_T^2}{n E t_s^3 a^2} + \frac{Ma}{3EI_p} + \frac{Mb}{EI_P}\right)} = \frac{E}{\left(\frac{\beta h_T^2}{n t_s^3 a^2} + \frac{a}{3I_P} + \frac{b}{I_P}\right)} \quad (5)$$

when the contact is at the flange-lip junction line.

4. Results validated by experimental data

The results recorded from the *F*-tests have been used to validate the analytical model presented above. Typical moment–rotation curves from both test results and analytical predictions are presented in Fig. 15. As in Fig. 5, almost all curves show a notable linear feature during the entire loading range apart from Z30720FD. This suggests that a constant rotation stiffness employed for the purlin–sheeting interaction design is essentially valid. The analytical calculation results for rotational stiffness are compared to the experimental data and summarised in Table 5. It is worth noting that the inclinometers that are used to measure the rotational angles are fixed near the flange-web corner. Although in the test, they have been fixed as close to the corner as possible, it is inevitable that there will be an offset distance *e* between the centre and corner. To allow for that, in calculating C_d, the additional angle developed between the corner and inclinometer centre is considered by adding a term of e/I_p to the denominator in both Eqs (4) and (5).

It can be seen that consistently good agreement is achieved between the test and prediction results, which suggests that the analytical model can predict sufficiently accurate results for rotational stiffness. It is noted that the analytical model is a linear model as can be seen from the derivation process. The test/prediction ratios from Table 5 have a standard deviation of 0.05 and a maximum difference of 11%.

The last column in Table 5 shows the ratio of rotational stiffness between FU and FD, and it can be seen that the rotational stiffness in the FU condition is greater than that in the FD condition in all cases regardless of the purlin's geometry. The FD/FU ratio ranges from 0.72 to 0.92. This trend also agrees with the results based on the EC3 model [19]. The cause of this trend can be easily explained by the additional term in the analytical model, i.e., Eq. (3b). The term that causes the difference is b/EI_p, which indicates that a purlin with a smaller *b* value or a larger thickness is likely to produce a notable difference under FD and FU conditions.

The contribution of θ_l and θ_p to the overall rotation for sigma sections is presented in Figs. 16 and 17, for the FD and FU conditions, respectively. In the FD condition, the proportion of θ_l ranges from 35% to 78% for 200 series sections, from 50% to 87% for 240 series sections and from 55% to 86% for 300 series sections. In the FU condition, this proportion has risen to 48–88% for 200 series, 62–92% for 240 series and 69–96% for 300 series. In each series, this proportion will increase with the purlin thickness. This trend agrees with the fact that θ_l is due to the sheet deformation, while θ_p is due to the purlin flange panel deformation. The effect of flange width on the proportion of θ_l can also be observed from Figs. 16 and 17. For instance, from section groups Σ20025/Σ30025 to Σ24030/Σ30030, the flange width rises from 62.5 mm to 75 mm, but the θ_l proportion in the FD condition varies from 79%/74% to 88%/86% and in the FU condition, from 88%/86% to 93%/95%. Therefore the effect of the flange width can be treated as insignificant. Similar patterns are found for the Z sections as shown in Figs. 18 and 19.

5. Parametric study

Studies [17,24] have found that the rotational stiffness of the purlin–sheet system depends on factors such as the shape and thickness of the sheet, the cross-section of the purlin, the number of screws per unit length and the connection details. The analytical model developed in this paper has taken account of these factors, and therefore it can be used for parametric studies. As discussed in the proceeding section, θ_l and θ_p are related to the sheet thickness and purlin thickness, respectively. A group of sigma sections

Table 6
Summary of geometrical details of Σ24030FD specimen and sheeting.

Purlin section	Web depth (mm)	Flange width (mm)	t_s (mm)	t_p (mm)	a (mm)	b (mm)	b_T (mm)	h_T (mm)	S (mm)	L (mm)
Σ24030	240	62.5	0.7	2.99	31.25	31.25	130	65	200	1000

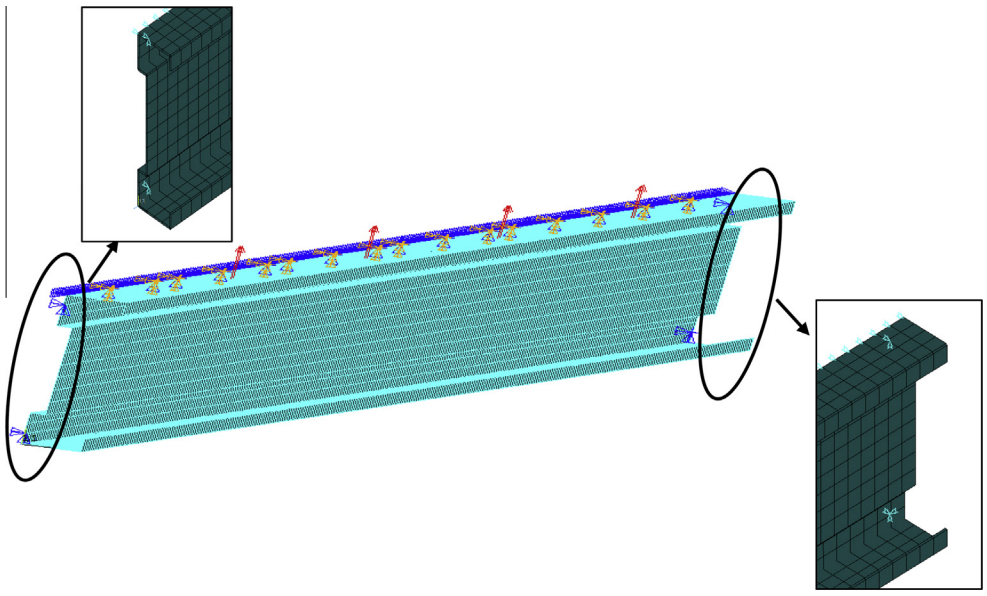

Fig. 22. FE model for Σ24030 purlin under the uplift load.

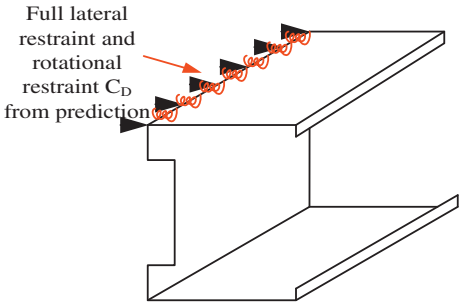

Fig. 23. Spring configurations in FEA model.

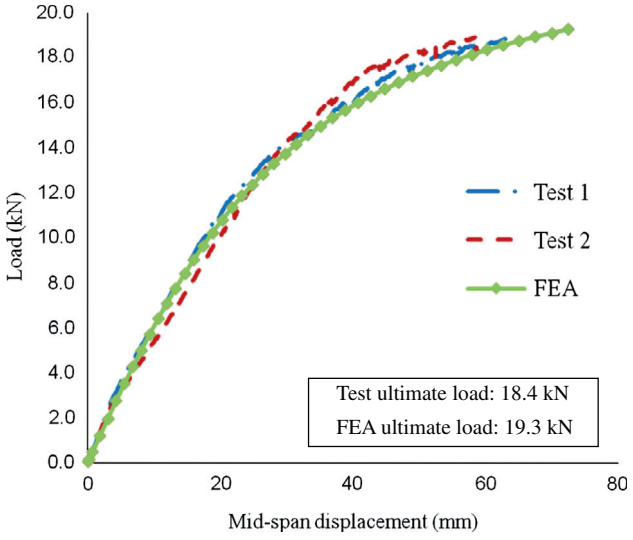

Fig. 25. Load–displacement curves.

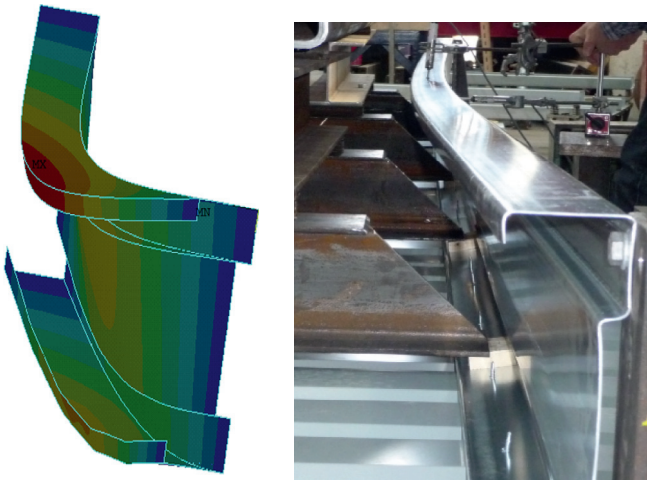

(a) Numerical model (b) Experiemetal observation

Fig. 24. Comparison of the deformation between the numerical and experimental results.

with a depth 240 mm and under the FD condition have been chosen as an example for parametric analysis. In Fig. 20, θ_l versus the sheet thickness curves for purlin sections of 3 mm with various flange widths, i.e. 62.5, 65, 75, 100 mm respectively, is presented. Similarly, Fig. 21 presents θ_p versus the purlin thickness curves for the same range of flange widths. Based on the results, the following observations can be made:

(1) θ_l declines with an increase in sheet thickness. The effect of sheet thickness on θ_l is more notable for small t_s values, specifically, less than 0.6 mm. The variation in θ_l caused by different flange widths C is inconclusive.
(2) The effect of purlin thickness on θ_p has a similar trend to that of sheet thickness on θ_l. Additionally, when the purlin thickness is up to 1.5 mm, this type of effect is particularly significant. The effect of flange width is only noticeable when the purlin thickness is rather small, e.g. up to 1.5 mm.

6. Application of the developed model in numerical simulation

One of the test specimens, Σ24030FD, is considered as a worked example to demonstrate the application of the above-developed model. For the ease of reference, the geometrical details of both purlin and sheeting are listed in Table 6. The Young's modulus for both purlin and sheeting is E = 210 GPa and the Possion ratio v = 0.3. Five screws are used within a length of 1 m, i.e. n = 5.

The second moment of area of purlin $I_p = Lt_p^3/12(1-v^2) = 1000\times 2.99^3/12(1-0.3^2) = 2448$ m^4; coefficient β for screw at the mid-point of sheeting trough: β = 0.078. Therefore, the rotational stiffness is:

$$C_D = \frac{E}{\left(\frac{\beta h_T^2}{nt_s^3 a^2}+\frac{a}{3I_p}+\frac{b}{I_p}\right)} = \frac{2.1\times 10^5}{\left(\frac{0.078\times 62.5^2}{5\times 0.7^3\times 31.25^2}+\frac{31.25}{3\times 2448}+\frac{31.25}{2448}\right)}$$
$$= 1055569 \text{ N mm/rad/m} = 1056 \text{ N m/rad/mm}$$

This result is higher than that listed in Table 5, i.e. 939 N m/rad/mm as it considers the rotation being measured exactly at the flange-web junction line.

The rotational stiffness is often considered in analysing the sheeting–purlin interaction [16–18,25–27]. Due to the complex nature of purlin–sheeting systems, most FEA models choose lateral and/or rotational spring elements as a substitute for the actual interactional effect. Such types of purlin/sheeting interaction are realised through the compression from the contact surface between the purlin flange and sheeting and the tension in the screw connections, under an external loading. It is this tension effect that provides the compression flange an effective restraint in the lateral direction.

The rotational stiffness derived can be applied directly in an FEA model. A numerical model is developed by using ANSYS [28] to illustrate the treatment of purlin/sheeting interaction. The model is for a 6-m simply-supported single span purlin made of Σ24030 subjected to a series of multi-point uplift loads, which has been tested by Yang and Liu [3]. The meshing and the application of boundary conditions are shown in Fig. 22. The effect of sheeting is simulated by applying lateral and rotational spring elements on the compression flange-web junction line. An illustration of spring configurations is provided in Fig. 23. The lateral restrain is set to be fully effective and the rotational spring is assigned with a stiffness based on the above calculation. The meshing density is determined through a convergence analysis. Other parameters such as the material properties, boundary conditions and geometry are set based on the measurement of the actual specimen.

By performing a non-linear inelastic analysis using this numerical model, the failure deformation of purlin is captured and shown in Fig. 24 along side with the picture taken in the test. A close agreement can be seen from the comparison. The applied load vs. the mid-span displacement curves from both lab test and numerical modelling are presented to show the comparison in Fig. 25. Again, a satisfactory agreement has been observed.

7. Conclusion

An analytical method to predict the rotational stiffness for cold-formed zed and sigma purlin/sheeting systems is reported in this study. This new method considers the interactional effect at screw points as well as the effect of loading directions. It is found that the rotational stiffness is higher when the purlin is in contact with the sheet at the flange-web junction line than when the purlin touches the sheet at the flange-lip junction line. One of the reasons causing this trend is that the latter case tends to have a shorter lever-arm, resulting in a high tensile force in the screws and hence a larger rotation. The method has been validated by a series of F-tests on both zed and sigma sections. A good agreement between the experimental and analytical results (i.e., with an average difference of 4%) has been observed. The method provides a simplified means to predict the rotational stiffness with high accuracy. This type of parameter is often required in FEA modelling for CFS roof systems. This is a key step forward in developing a design method for metal buildings with light steel roof and wall systems.

Acknowledgement

This research was carried out with the laboratory facilities provided by the University of Birmingham and financial support provided by the UK Engineering and Physical Science Research Council (EPSRC). The authors gratefully acknowledge the test specimens provided by Albion Sections Ltd. The second author is also grateful for the funding provided by the State Key Laboratory of Ocean Engineering, Shanghai Jiao Tong University, PR China.

Appendix A

A Levy's solution can be obtained by considering the above plate model.

$$w = \sum_{m=1}^{\infty} Y_m \sin\left(\frac{m\pi x}{b_T}\right) \tag{A1}$$

where m = 1, 3, 5…, n, and

$$Y_m = A_m \cosh\left(\frac{m\pi y}{b_T}\right) + B_m\left(\frac{m\pi y}{b_T}\right)\sinh\left(\frac{m\pi y}{b_T}\right) + C_m \times \sinh\left(\frac{m\pi y}{b_T}\right) + D_m\left(\frac{m\pi y}{b_T}\right)\cosh\left(\frac{m\pi y}{b_T}\right) \tag{A2}$$

For a plate with two opposite edges simply supported and the other two fixed (S–F–S–F), the constants can be solved as:

$$A_m = \frac{b_T F(-1)^{\frac{m+1}{2}}\left[-4b_T^2\cosh\left(\frac{m\pi h_T}{2b_T}\right)^2 + m^2\pi^2 h_T^2 + 4b_T^2\right]}{4\left[m\pi h_T + 2b_T\sinh\left(\frac{m\pi h_T}{2b_T}\right)\cosh\left(\frac{m\pi h_T}{2b_T}\right)\right]m^3\pi^3 D}$$

$$B_m = \frac{b_T^3 F(-1)^{\frac{m+1}{2}}\left[1-\cosh\left(\frac{m\pi h_T}{2b_T}\right)^2\right]}{\left[m\pi h_T + 2b_T\sinh\left(\frac{m\pi h_T}{2b_T}\right)\cosh\left(\frac{m\pi h_T}{2b_T}\right)\right]m^3\pi^3 D}$$

$$C_m = \frac{(-1)^{\frac{m+1}{2}} b_T^2 F}{m^3\pi^3 D}\left\{\mathrm{H}(y) - \frac{\left[2b_T\sinh\left(\frac{m\pi h_T}{2b_T}\right)\cosh\left(\frac{m\pi h_T}{2b_T}\right) + m\pi h_T\right]}{2\left[m\pi h_T + 2b_T\sinh\left(\frac{m\pi h_T}{2b_T}\right)\cosh\left(\frac{m\pi h_T}{2b_T}\right)\right]}\right\}$$

$$D_m = \frac{(-1)^{\frac{m+1}{2}} h_T^2 F}{m^3\pi^3 D}\left(\frac{1}{2} - \mathrm{H}(y)\right) \tag{A3a-d}$$

For engineering applications, m = 5 can be deemed to produce sufficiently accurate results. H(y) represents the Heaviside function, i.e. H(y) = 0 for y < 0 and H(y) = 1 for $y \geqslant 0$. The resolved constants can be substituted into Eq. (A1) to calculate the deflection caused by local sheet deformation.

References

[1] Liu Q, Yang J, Li LY. Pseudo-plastic moment resistance of continuous beams with cold-formed Sigma section sat internal supports: experimental study. Eng Struct 2011;33:947–57.
[2] Rhodes J, Lawson RM. Design of structures using cold formed steel sections. Ascot: The Steel Construction Institute; 1992.
[3] Yang J, Liu Q. An experimental study into flexural behaviour of sigma purlins attached with roof sheets. Eng Struct 2012;45:481–95.
[4] Lucas RM, AlBermani FGA, Kitipornchai S. Modelling of cold-formed purlin–sheeting systems. 1. Full model. Thin-Wall Struct 1997;27(3):223–43.
[5] Lucas RM, AlBermani FGA, Kitipornchai S. Modelling of cold-formed purlin–sheeting systems. 2. Simplified model. Thin-Wall Struct 1997;27(4):263–86.

[6] Vieira LCM et al. Numerical analysis of cold-formed steel purlin–sheeting systems. In: Fifth international conference on thin-walled structures, Brisbane, Australia; 2008.
[7] Vieira Jr LCM et al. Simplified models for cross-section stress demands on C-section purlins in uplift. Thin-Wall Struct 2010;48(1):33–41.
[8] Li LY et al. Theoretical analysis of partially restrained zed-purlin beams subjected to up-lift loads. J Constr Steel Res 2012;70:273–9.
[9] Sokol L. Stability of cold formed purlins braced by steel sheeting. Thin-Wall Struct 1996;25(4):247–68.
[10] Vrany T. Effect of loading on the rotational restraint of cold-formed purlins. Thin-Wall Struct 2007;44(12):1287–92.
[11] Yang J, Liu Q. Sleeve connections of cold-formed steel sigma purlins. Eng Struct 2012;43:245–58.
[12] Ye ZM et al. Buckling behaviour of cold-formed zed-purlins partially restrained by steel sheeting. Thin-Wall Struct 2002;40(10):853–64.
[13] Ye ZM, Kettle R, Li LY. Analysis of cold-formed zed-purlins partially restrained by steel sheeting. Comput Struct 2004;82(9–10):731–9.
[14] Schafer BW. Review: the direct strength method of cold-formed steel member design. J Constr Steel Res 2008;64(7–8):766–78.
[15] Fiorino L et al. Experimental tests on typical screw connections for cold-formed steel housing. Eng Struct 2007;29(8):1761–73.
[16] Katnam KB et al. A theoretical numerical study of the rotational restraint in cold-formed steel single skin purlin–sheeting systems. Comput Struct 2007;85(15–16):1185–93.
[17] Katnam KB et al. Modelling of cold-formed steel sandwich purlin–sheeting systems to estimate the rotational restraint. Thin-Wall Struct 2007;45(6):584–90.
[18] Vrany T. Torsional restraint of cold-formed beams provided by corrugated sheeting for arbitrary input variables. In: Eurosteel – the third European conference on steel structures, Coimbra, Portugal; 2002.
[19] BSI. BS EN 1993-1-3: 2006. Design of steel structures-cold formed structures. Special considerations for purlins, liner trays and sheetings; 2006 [chapter 10].
[20] Lindner J, Gregull T. Torsional restraint coefficients of profiled sheeting. IABSE colloquium thin-walled metal structures in buildings. Stockholm; 1986.
[21] AISI. North American specification for the design of cold-formed steel structural members. AISI S100-2007; 2007.
[22] Gao T, Moen C. Predicting rotational restraint provided to wall girts and roof purlins by through-fastened metal panels. Thin-Wall Struct 2012;61:145–53.
[23] Timoshenko S, Wojnowski-Kreiger S. Theory of plates and shells. New York and London: McGraw-Hill; 1959.
[24] Xu YL, Reardon R. Test of screw fastened profiled roofing sheets subject to simulated wind uplift. Eng Struct 1993;15(6):423–30.
[25] Liu Q, Yang J, Li LY. Pseudo-plastic moment resistance of continuous beams with cold-formed sigma sections at internal supports: an experimental study. Eng Struct 2011;33(3):947–57.
[26] Rousch CJ, Hancock GJ. Comparison of tests of bridged and unbridged purlins with a non-linear analysis model. J Constr Steel Res 1997;41(2–3):197–220.
[27] Liu Q, Yang J, Chan AHC, Li LY. Pseudo-plastic moment resistance of continuous beams with cold-formed Sigma sections at internal supports: a numerical study. Thin-Wall Struct 2011;49:1592–604.
[28] ANSYS. Commands reference, elements reference, operation guide, basic analysis guide, theory reference for ANSYS; 2007.